CrossMark

The Binary Mass Ratio in the Black Hole Transient MAXI J1820+070

M. A. P. Torres[1,2] , J. Casares[1,2] , F. Jiménez-Ibarra[1,2] , A. Álvarez-Hernández[1,2] , T. Muñoz-Darias[1,2] , M. Armas Padilla[1,2],
P. G. Jonker[3,4] , and M. Heida[5]

[1] Instituto de Astrofísica de Canarias, E-38205 La Laguna, Tenerife, Spain
[2] Departamento de Astrofísica, Universidad de La Laguna, E-38206 La Laguna, Tenerife, Spain
[3] SRON, Netherlands Institute for Space Research, Sorbonnelaan 2, NL-3584 CA Utrecht, The Netherlands
[4] Department of Astrophysics/IMAPP, Radboud University, P.O. Box 9010, 6500 GL Nijmegen, The Netherlands
[5] ESO, Karl-Schwarzschild-Str 2, D-85748 Garching bei München, Germany

Abstract

We present intermediate-resolution spectroscopy of the optical counterpart to the black hole X-ray transient MAXI J1820+070 (=ASASSN-18ey) obtained with the OSIRIS spectrograph on the 10.4 m Gran Telescopio Canarias. The observations were performed with the source close to the quiescent state and before the onset of renewed activity in 2019 August. We make use of these data and K-type dwarf templates taken with the same instrumental configuration to measure the projected rotational velocity of the donor star. We find $v_{\rm rot} \sin i = 84 \pm 5$ km s^{-1} (1σ), which implies a donor to the black hole mass ratio $q = M_2/M_1 = 0.072 \pm 0.012$ for the case of a tidally locked and Roche-lobe filling donor star. The derived dynamical masses for the stellar components are $M_1 = (5.95 \pm 0.22)\sin^{-3} i\ M_\odot$ and $M_2 = (0.43 \pm 0.08)\sin^{-3} i\ M_\odot$. The use of q, combined with estimates of the accretion disk size at the time of the optical spectroscopy, allows us to revise our previous orbital inclination constraints to $66° < i < 81°$. These values lead to 95% confidence level limits on the masses of $5.73 < M_1(M_\odot) < 8.34$ and $0.28 < M_2(M_\odot) < 0.77$. Adopting instead the $63° \pm 3°$ orientation angle of the radio jet as the binary inclination leads to $M_1 = 8.48^{+0.79}_{-0.72} M_\odot$ and $M_2 = 0.61^{+0.13}_{-0.12}\ M_\odot$ (1σ).

Unified Astronomy Thesaurus concepts: Stellar mass black holes (1611); Low-mass x-ray binary stars (939)

1. Introduction

MAXI J1820+070 (hereafter J1820) is an X-ray transient discovered by the MAXI mission at the rise of its 2018 March outburst (Kawamuro et al. 2018). The source was soon after classified as a transient black hole (BH) candidate in the low-hard state in light of the multiwavelength and variability properties (Baglio et al. 2018; Kawamuro et al. 2018; Kennea et al. 2018; Shidatsu et al. 2019). The source later moved to the soft state (e.g., Fabian et al. 2020). During the state transition, a change on the type of X-ray quasi-periodic oscillations was observed and immediately followed by the launch of a relativistic jet (Bright et al. 2020; Homan et al. 2020).

The spectrum of the optical counterpart (ASASSN-18ey; Denisenko 2018; Tucker et al. 2018) displayed emission lines typical of low-mass X-ray binaries in an outburst with marked disk wind profile components (Muñoz-Darias et al. 2019). An optical modulation with a period of 16.87 ± 0.07 hr was found from intense photometric monitoring during the early outburst phase, and interpreted as a superhump (Patterson et al. 2018). Multiband counterparts were identified in prediscovery images of the field (Baglio et al. 2018; Denisenko 2018; Tucker et al. 2018). The optical counterpart is sufficiently bright to deliver a parallax determination in GAIA DR2 (e.g., Atri et al. 2019; Gandhi et al. 2019), and historic outburst episodes have been detected through analysis of photographic plates taken in 1898 and 1934 (Kojiguchi et al. 2019). Radio astrometric observations of the gigahertz counterpart has provided a trigonometric parallax that yields a direct distance measurement toward J1820 of 2.96 ± 0.33 kpc and an inclination to the line of sight for the jet ejecta of $63° \pm 3°$ (Atri et al. 2020).

The radial velocity curve of the donor star in J1820 was derived from data acquired during episodes of fading activity that took place in 2019 February and June, when the optical counterpart dimmed close to the pre-outburst brightness (Torres et al. 2019). The measured mass of the compact object exceeds $5.2\,M_\odot$, placing J1820 among the dynamically established stellar-mass BHs, with only less than 20 known in the Galaxy (Casares & Jonker 2014; Corral-Santana et al. 2016). The spectroscopic orbital period found from the radial velocities was a few percent shorter than the photometric period reported by Patterson et al. (2018), confirming the occurrence of superhumps during outburst. The prompt determination of the orbital ephemeris also permitted us to conclude that at least one X-ray dipping episode observed during the outburst (Kajava et al. 2019; see also Homan et al. 2018) took place at an orbital phase where absorption by the outer disk bulge is expected. Torres et al. (2019) set the first limits on the binary orbital inclination to $69° \lesssim i \lesssim 77°$. These constraints were obtained by considering the absence of X-ray eclipses during the outburst, the detection of a disk grazing eclipse by the donor star in the Hα line, and a provisional value for the mass ratio of $q \simeq 0.12$. The latter was an estimate obtained from the empirical relationship between q and the orbital period to superhump period excess found for cataclysmic variables.

In this Letter we present new optical spectroscopy of J1820 that leads to a direct and accurate determination of q. The performed analysis and results are outlined as follows: Section 2 describes the observations and the data reduction steps. In Section 3.1 we measure the projected rotational broadening of the photospheric lines from the donor star and q. The value of q is utilized in Section 3.2 to set constraints on the accretion disk outer radius and revise the limits for the binary system inclination. Finally, in Section 4 we discuss our results.

Table 1
Journal of the J1820 OSIRIS Observations

Date (2019)	Orbital[a] Phase	Exp. (#)	Seeing[b] ('')	r (mag[c])
29 Jul	0.28–0.32	3	0.7–1.2	17.8–17.5
3 Aug	0.50–0.53	3	0.8–1.0	17.6–17.4
7 Aug	0.36–0.39	3	0.8–0.9	17.4

Notes.
[a] According to the ephemeris in Torres et al. (2019).
[b] FWHM of the spatial profile at spectral positions near $\lambda 6410$.
[c] Photometry calibrated with field stars in Pan-STARRS (Chambers et al. 2016).

2. Observations and Data Reduction

The data presented in this Letter were obtained with the 10.4 m Gran Telescopio Canarias (GTC) at the Observatorio del Roque de los Muchachos on La Palma, Spain. The observations were performed with the OSIRIS spectrograph (Cepa et al. 2000) across three different nights in 2019 July and August, when J1820 was near the quiescent state. In Table 1 we provide the seeing conditions and the r-band apparent magnitude of the optical counterpart. The former was measured from the spatial profile of the spectra and the latter from the OSIRIS acquisition images. The table also gives the orbital phases at the time of the observations.

We used grism R2500R to cover the 5575–7685 Å wavelength range with a 0.5 Å pix^{-1} dispersion (unbinned detector). All observations were carried out with a 0$\rlap{.}''$4 wide slit in order to secure a slit-limited resolution of 2.0 Å FWHM (90 km s^{-1} at Hα). In total we were able to collect nine 900 s spectra of J1820 before it resumed outburst activity. In order to evaluate the line rotational broadening from these data, high signal-to-noise ratio exposures of stars HD 219134 (K3 V), HD 216803 (K4 V), and 61 Cyg A (K5 V) were performed under slit-limited conditions using the same instrumental setup as for J1820. Finally, HgAr+Ne comparison arc lamp spectra were taken at the end of each observing night.

The spectra were reduced, extracted, and wavelength-calibrated following standard techniques implemented in IRAF. The pixel-to-wavelength scale was determined through third-order spline fits to 12 arc lines. The rms scatter of the fits was always <0.01 Å. We made use of the [O I] 6300.3 Å sky emission line to correct for wavelength zero-point deviations, which were <19 km s^{-1}.

3. Analysis and Results

To perform the analysis detailed in this section we made use of MOLLY- and PYTHON-based software. Unless otherwise stated, to evaluate the 1σ uncertainty in q and other quantities we applied a Monte Carlo approach where we draw 10,000 random values from normal distributions defined by the mean value and 1σ errors of the measurements in play. We also employed the ephemeris and orbital elements given by Torres et al. (2019) since they were not significantly improved by the inclusion of radial velocities derived from the data under discussion. Finally, for the analytical expressions of the representative accretion disk radii calculated in Section 3.2 we refer the reader to the reviews by Warner (1995) and Frank et al. (2002).

3.1. Projected Rotational Velocity and Binary Mass Ratio

The motivation for the spectroscopic observations was to firmly determine the binary mass ratio in J1820. To do this, we take advantage of the fact that the tidal interactions between the BH and mass-donor star are able to align orbital and stellar spin axes, circularize the orbit, and synchronize the stellar rotation with the orbital motion. These three changes take place on timescales much shorter than the lifetime of the binary (see, e.g., Zahn 1977; Tassoul 1988). Thus, the rotational broadening of the star, projected onto our line of sight, is $v_{\rm rot} \sin i \approx K_2 (1 + q) R_2 / a$, where i is the binary inclination, K_2 the radial velocity semi-amplitude of the donor star, and R_2 / a the ratio between the Roche-lobe effective radius of the donor star and the separation between the stellar components. R_2 / a can be expressed as a function of q only (Eggleton 1983) and, therefore, the projected rotational velocity of the donor star is approximated to $v_{\rm rot} \sin i \approx 0.49 (1 + q) q^{2/3} K_2 [0.6 q^{2/3} + \ln(1 + q^{1/3})]^{-1}$. Hence q can be simply derived by measuring K_2 and $v_{\rm rot} \sin i$. The latter quantity is imprinted in the spectra by Doppler broadening of the donor star photospheric features.

To measure $v_{\rm rot} \sin i$ we employ the optimal subtraction technique described in Marsh et al. (1994; see also Steeghs & Jonker 2007). This technique relies on finding the smallest residual after subtracting a set of spectral templates (artificially broadened and scaled to match the width and depth of the photospheric lines in the donor star) from the Doppler-corrected average spectrum of the target. Our templates are the spectra of the three K-type dwarfs observed with OSIRIS (Section 2), which have $v_{\rm rot} \sin i \lesssim 2$ km s^{-1} and spectral types close to that estimated for the donor in J1820.

Following Torres et al. (2019), we perform the analysis in the spectral range 5200–6815 Å, excluding regions containing emission lines or telluric or interstellar absorptions. The data were rebinned onto a logarithmic wavelength scale and their continua normalized to unity. The latter step was performed by dividing each spectrum by a third-order spline fit to the continuum. Radial velocity shifts between the nine normalized J1820 spectra, and each spectral template was calculated by cross-correlation of features in the above wavelength interval. Each J1820 spectrum was then Doppler-corrected to the rest frame of the template star by subtracting the corresponding radial velocity. The Doppler-corrected spectra were averaged assigning different weights to the individual spectra to maximize the signal-to-noise ratio in the resulting sum. In order to account for the radial velocity drift experienced by the stellar features during the exposures, due to the orbital motion of the donor star, we simulated the effect by making nine copies of each template, which were smeared considering the length of the exposures and the orbital ephemeris (see, e.g., Torres et al. 2002b for details). The smeared template copies were then summed using identical weights as for the J1820 spectra.

The three summed spectral templates were broadened from 1 to 150 km s^{-1} in steps of 1 km s^{-1} through convolution with the rotational profile of Gray (1992). We used limb-darkening coefficients of 0.67, 0.69, and 0.71 for the K3 V, K4 V, and K5 V templates, respectively (Claret et al. 1995)—use of a lower limb-darkening coefficient (of 0.5) decreases the $v_{\rm rot} \sin i$ values reported in this work by < 3 km s^{-1}. The gravity darkening and the Roche-lobe geometry of the donor star are not accounted for since the statistical uncertainties are
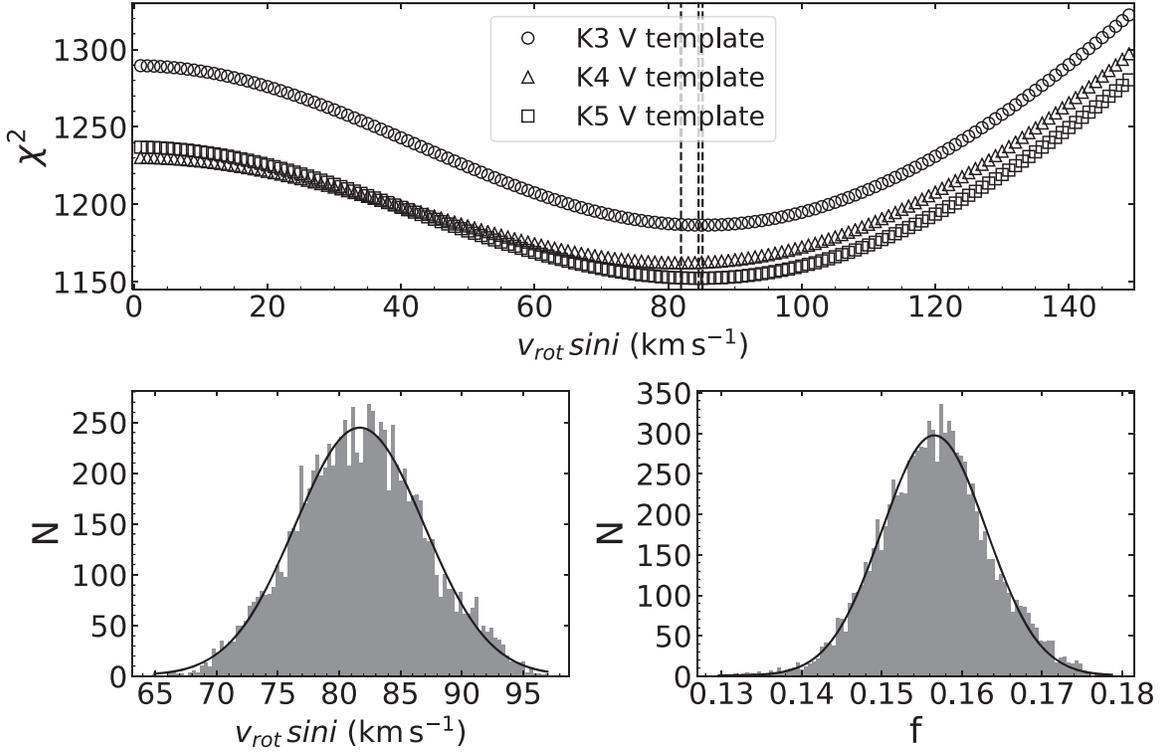
Figure 1. Top: χ^2 statistics as a function of the $v_{\rm rot} \sin i$ applied to the K-type dwarf templates for its optimal subtraction from the average J1820 spectrum (degrees of freedom = 997). Bottom: distribution of $v_{\rm rot} \sin i$ values (left) and corresponding f values (right) obtained by subtracting the K4 V template from 10,000 bootstrap copies of the J1820 average spectrum. Gaussian fits to the distributions are shown. They deliver $v_{\rm rot} \sin i = 82 \pm 5$ km s^{-1} and $f = 0.158 \pm 0.007$ at the 68% confidence level.

dominant over the effect they introduce in the measurement of q. With respect to this, see Section 3.2 in Marsh et al. (1994) for a thorough investigation of their impact on the evaluation of q for the BH transient A0620–00.

The broadened templates were subtracted from the J1820 average spectrum while optimizing for a variable scaling factor f that represents the fractional contribution of light from the donor star to the total light in the binary system. The final values for $v_{\rm rot} \sin i$ and f in J1820 were established by minimizing the χ^2 statistics between the residual of the subtraction and a smoothed version of itself. Figure 1 shows for each template the resulting χ^2 as function of the applied broadening. The three χ^2 curves give single minima that yield consistent values of the optimal $v_{\rm rot} \sin i$. To evaluate the uncertainties, we repeat the above optimal subtraction procedure and χ^2 minimization in 10,000 bootstrap copies of the J1820 average spectrum. All resulting distributions of $v_{\rm rot} \sin i$ and f were satisfactorily described with a Gaussian model and we adopt their mean and standard deviation as reliable estimates of their value and 1σ uncertainty. The results for each template are given in Table 2. The χ^2 minimization also shows that the donor star in J1820 contributes ~16%–17% to the total flux. This is accordant with the contribution found in the data taken in 2019 June (Torres et al. 2019).

From the above results, we take $v_{\rm rot} \sin i = 84$ km s^{-1}, and a 1σ uncertainty of 5 km s^{-1}, combined with $K_2 = 417.7 \pm 3.9$ km s^{-1}, yields $q = 0.072 \pm 0.012$ (1σ). We note here that a similar result ($v_{\rm rot} \sin i = 81 \pm 8$ km s^{-1}) is achieved when applying this analysis to the higher-resolution ISIS spectra in Torres et al. (2019), despite being taken under variable seeing-limited conditions.

Table 2
Optimal Subtraction Results (1σ Errors)

Template	Spectral Type	$v_{\rm rot} \sin i$ (km s^{-1})	f
HD 222237	K3 V	85 ± 5	0.173 ± 0.008
HD 216803	K4 V	82 ± 5	0.158 ± 0.007
61 Cyg A	K5 V	85 ± 5	0.17 ± 0.01

3.2. Outer Disk Radius and Binary Inclination

The analysis above has supplied us with a solid measurement of q that, in combination with information on the outer disk radius, can serve to improve on the estimates of the binary inclination.

On the basis of geometrical arguments, the nondetection of X-ray eclipses during the outburst implies an upper limit to the binary inclination of $\cos i \geqslant R_2/a = 0.49 q^{2/3}[0.6 q^{2/3} + \ln(1 + q^{1/3})]^{-1}$. This condition yields $i < 80°\!.8$ (3σ). On the other hand, the detection of a grazing eclipse of the disk by the donor star sets a lower limit to the inclination of $\cos i \leqslant R_2/(a - R_{\rm d})$ with $R_{\rm d}$ being the outer disk radius. This condition can be conveniently rewritten as

$$\cos i \leqslant \frac{0.49 q^{\frac{2}{3}}[0.6 q^{\frac{2}{3}} + \ln(1 + q^{\frac{1}{3}})]^{-1}}{1 - \left[\frac{1}{2} - 0.227 \log_{10}(q + 0.01)\right]\left(\frac{R_d}{b_1}\right)} \quad (1)$$

by giving $R_{\rm d}$ relative to the inner Lagrangian point distance to the BH (b_1) and b_1/a in function of q, following the approximation in Equation (A2) of Ziółkowski & Zdziarski

(2018). Thus, knowledge of q and R_d/b_1 constrains i. Estimates of R_d exist for three BH X-ray transients in quiescence. These were established from detection in Hα Doppler tomograms of a well-resolved and confined hotspot caused by the impact of the gas stream (from the donor star) with the outer disk regions. These tomograms show that R_d/b_1 is 0.50 ± 0.05 both in A 0620-00 ($q = 0.067 \pm 0.01$; Marsh et al. 1994) and Nova Muscae 1991 ($q = 0.079 \pm 0.007$; Peris et al. 2015), while $R_d/b_1 = 0.47 \pm 0.03$ in GS 2000+25 ($q = 0.042 \pm 0.012$; Casares et al. 1995). An Hα tomogram performed for J1820 by phase folding the data obtained in 2019 June–August on the orbital period did not lead to the detection of a hotspot. Based on the tomograms of the above three quiescent BH binaries, we adopt $R_d^{quie}/b_1 \sim 0.5$ for J1820 in quiescence, a value that is near the stream circularization radius $R_{circ}/b_1 = (1 + q)(b_1/a)^3 = 0.45$. Presumably, at the time of the spectroscopic detection of the grazing eclipse in J1820, the disk was larger than in true quiescence since the system was still fading in brightness. This can be tested by using the FWHM of the Hα emission line as a proxy of the disk size. Thus, we calculate an expected Hα FWHM^{quie} of 1793 ± 101 km s^{-1} for J1820 in true quiescence using the empirical relation $K_2 = (0.233 \pm 0.013) \times$ FWHM^{quie} found for quiescent BH transients (Casares 2015). Following the procedures outlined by this author, we measure the Hα FWHM in the spectroscopy presented in Torres et al. (2019). We derive a FWHM of 1614 km s^{-1} and standard deviation of 96 km s^{-1} by fitting a single Gaussian model to the individual normalized line profiles while correcting for the instrumental broadening. Assuming an $r^{-1/2}$ rotational (Keplerian) velocity law for the disk, we obtain $R_d/R_d^{quie} = (\text{FWHM}^{quie}/\text{FWHM})^2 = 1.2 \pm 0.2$. This implies $R_d \sim (0.60 \pm 0.10)b_1 = (0.74 \pm 0.12)R_l$ at the time of the grazing eclipse detection. Here R_l is the equivalent radius of the compact object's Roche lobe. Admittedly, this calculation does not allow us to set a stringent value for R_d and we are left with imposing limits to this quantity and i by employing characteristic accretion disk radii. A lower limit to i comes from the maximum reachable disk radius caused by tidal truncation: $R_T = 0.6/(1 + q)a = 0.75b_1 = 0.93R_l$. On the other hand, during the outburst the disk had to expand to or beyond the 3:2 resonance radius (resonance near the 3:1, $k = 2$ commensurability) $R_{32} = 0.63b_1 = 0.78R_l$, a condition that drives the superhump phenomena (e.g., Whitehurst & King 1991). Given that these analytically inferred radii are solely dependent on q, the evaluation of Equation (1) was performed through Monte Carlo randomization with q treated as being normally distributed. This yielded normalized distributions for i from which we obtain 3σ lower limits of $61°9$, $66°2$, and $72°8$ for a disk radius equal to R_t, R_{32}, and R_{circ}, respectively. Therefore, from geometrical arguments alone we conservatively constrain i to be in the range $61°9$–$80°8$.

4. Discussion

The analysis of the OSIRIS spectroscopy (Section 3.1) has yielded $q = 0.072 \pm 0.012$, which is a factor ~ 2 lower than

the value estimated in our previous work by employing the relation between this binary parameter and the fractional superhump period excess $\Delta P = (P_{sh} - P_{orb})/P_{orb}$ (Torres et al. 2019). This discrepancy is most likely due to the use in the calculation of ΔP of the preliminary 0.703 ± 0.003 day superhump period (P_{sh}) provided in Patterson et al. (2018). An updated (but still provisional) period of 0.6903 ± 0.0003 days for the superhump was later reported by Patterson (2019) from further time-series photometry, while evidence for early evolution of P_{sh} was communicated by Variable Star Network observers that followed the 2018 outburst. Thus, a valid comparison between the result presented in this work and that obtainable through ΔP is subject to the publication of a rigorous study of the superhump temporal properties in J1820.

In Section 3.2 we constrain the binary inclination to be in the range $61°9 < i < 80°8$. These limits supersede the early restriction of $69° \lesssim i \lesssim 77°$ calculated by adopting an outer disk radius of $R_d \sim 0.5R_1$ and $q \simeq 0.12$ (Torres et al. 2019). On one hand, the allowed range for i encloses those expected for an X-ray dipper binary (Frank et al. 2002) and contains the $63° \pm 3°$ (1σ) inclination found for the radio jet (Atri et al. 2020). On the other hand, it excludes the $29.8^{+3.0}_{-2.7}$ (3σ) inclination for the inner disk obtained from modeling of X-ray spectra (Bharali et al. 2019). Still, we consider the new lower boundary of $61°9$ imposed by the disk tidal truncation radius not likely because the accretion disk should have contracted appreciably during the approach to quiescence. In fact, the Hα FWHM at the time of the grazing eclipse delivered a mean value of $R_d \sim 0.6b_1$ (Section 3.2) that is close to the 3:1 resonance radius ($R_{32} = 0.63b_1$). Thus, the grazing eclipse occurrence and standard deviation associated with the value of R_d evaluated from Hα can potentially be explained as caused by an asymmetric accretion disk extending to the resonance radius. In such a setting, the range of allowed inclinations narrows to $66° < i < 81°$. Support for this scenario could be provided by the photometric or spectroscopic detection of a precessing disk at the time of our observations or during early quiescence of the source (e.g., Torres et al. 2002a; Zurita et al. 2002).

Knowledge of K_2, the orbital period and q allows us to give the BH and donor star masses as a function of the binary inclination

$$M_1 = \frac{5.95 \pm 0.22}{\sin^3 i}M_\odot, \qquad M_2 = \frac{0.43 \pm 0.08}{\sin^3 i}M_\odot.$$

We display in Figure 2 the expected values of M_1 and M_2 obtained from both expressions for a given i with an assumed 1σ uncertainty of $1°$. Taking the favored constraint on the inclination ($66°2 < i < 80°8$) and the 1σ uncertainties in the above expressions, we derive the following ranges for the masses at 1σ:

$$5.96 < M_1(M_\odot) < 8.06, \quad 0.36 < M_2(M_\odot) < 0.66$$

and 2σ:

$$5.73 < M_1(M_\odot) < 8.34, \quad 0.28 < M_2(M_\odot) < 0.77.$$

The dipping behavior in J1820 was not as complex and copious as observed during the outburst of the 0.406 day orbital period BH candidate MAXI J1305-704 (Shidatsu et al. 2013), which has a close matching orbital period among known BH X-ray dippers. We take this difference as a supporting argument to
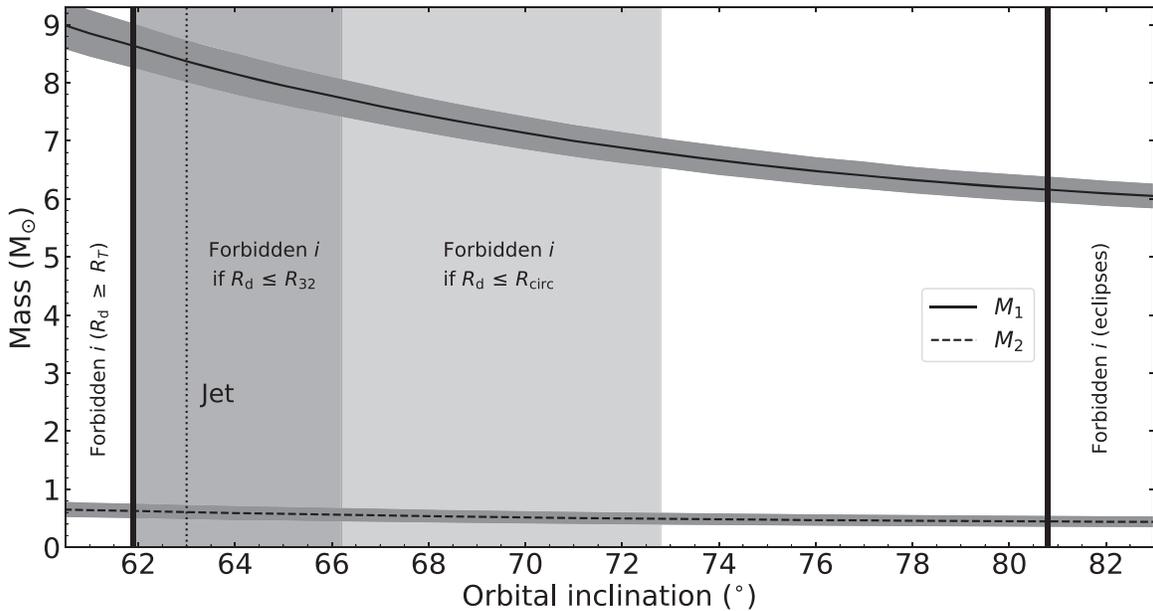
Figure 2. Possible values for the BH and donor mass (M_1 and M_2, respectively) as a function of the orbital inclination. The encompassing shaded regions show their 1σ uncertainties. The solid vertical lines mark extreme limits on the inclination: i must be $<80°\!\!.8$ since the system lacks X-ray eclipses, while $i > 61°\!\!.9$ is imposed by the condition that the disk size near quiescence shall not pass its tidal truncation radius, R_T. The dark-gray-shaded area marks impossible mass solutions if the outer disk radius R_d reached or exceeded the 3:1 resonance radius R_{32} at the time of the grazing eclipse detection with a minimum possible value for i of $66°\!\!.2$. The light-gray-shaded area represents impossible solutions if the accretion disk shrank to its circularization radius R_{circ}. In this case, the minimum possible i is $72°\!\!.8$. A vertical dashed line marks the inclination found for the radio jet.

prefer the low-end values in the range of possible binary inclinations found for J1820. This, in turn, points to large values of the permitted BH mass and to the less undermassive (evolved) donor star. It should be noted that the latter has spectral type K3–K5 and main-sequence stars with this spectral type have masses of $\sim 0.7\,M_\odot$.

We must stress here that the limits on i calculated in this work rest in the use of a simple model for the binary geometry that ignores the disk vertical structure and therefore they are subject to systematic effects. In this respect, the opening angle subtended by the accretion disk has been constrained observationally to $\leqslant 20°$ in neutron star low-mass X-ray binaries (see, e.g., Jiménez-Ibarra et al. 2018 and references therein). Hence, if we assume a similar angle for the disk in quiescent BH transients, the lower boundary on i will decrease such that the $63° \pm 3°$ (1σ) orientation angle for the jet ejecta (Atri et al. 2020) is fully compatible with being the binary inclination. If that was the case, we obtain values for the BH and donor star masses (at the 68% confidence level) of

$$M_1 = 8.48^{+0.79}_{-0.72}M_\odot, \qquad M_2 = 0.61^{+0.13}_{-0.12}M_\odot.$$

Modeling of the ellipsoidal modulation of the donor star expected in lightcurves obtained in the quiescence state may refute this possibility.

ORCID iDs

M. A. P. Torres ⬤ https://orcid.org/0000-0002-5297-2683
J. Casares ⬤ https://orcid.org/0000-0001-5031-0128
A. Álvarez-Hernández ⬤ https://orcid.org/0000-0002-0621-1293
T. Muñoz-Darias ⬤ https://orcid.org/0000-0002-3348-4035
P. G. Jonker ⬤ https://orcid.org/0000-0001-5679-0695
M. Heida ⬤ https://orcid.org/0000-0002-1082-7496

References

Atri, P., Miller-Jones, J. C. A., Bahramian, A., et al. 2019, MNRAS, 489, 3116
Atri, P., Miller-Jones, J. C. A., Bahramian, A., et al. 2020, MNRAS, 493, L81
Baglio, M. C., Russell, D. M., & Lewis, F. 2018, ATel, 11418, 1
Bharali, P., Chauhan, J., & Boruah, K. 2019, MNRAS, 487, 5946
Bright, J. S., Fender, R. P., Motta, S. E., et al. 2020, NatAs, in press (doi:10.1038/s41550-020-1023-5)
Casares, J. 2015, ApJ, 808, 80
Casares, J., Charles, P. A., & Marsh, T. R. 1995, MNRAS, 277, L45
Casares, J., & Jonker, P. G. 2014, SSRv, 183, 223
Cepa, J., Aguiar, M., Escalera, V. G., et al. 2000, Proc. SPIE, 4008, 623
Chambers, K. C., Magnier, E. A., Metcalfe, N., et al. 2016, arXiv:1612.05560
Claret, A., Diaz-Cordoves, J., & Gimenez, A. 1995, A&AS, 114, 247
Corral-Santana, J. M., Casares, J., Muñoz-Darias, T., et al. 2016, A&A, 587, A61
Denisenko, D. 2018, ATel, 11400, 1
Eggleton, P. P. 1983, ApJ, 268, 368
Fabian, A. C., Buisson, D. J., Kosec, P., et al. 2020, MNRAS, 493, 5389
Frank, J., King, A., & Raine, D. J. 2002, Accretion Power in Astrophysics (3rd ed.; Cambridge: Cambridge Univ. Press)

Gandhi, P., Rao, A., Johnson, M. A. C., Paice, J. A., & Maccarone, T. J. 2019, MNRAS, 485, 2642

Gray, D. F. 1992, The Observation and Analysis of Stellar Photospheres, Vol. 20 (Cambridge: Cambridge Univ. Press)

Homan, J., Altamirano, D., Arzoumanian, Z., et al. 2018, ATel, 11576, 1

Homan, J., Bright, J., Motta, S. E., et al. 2020, ApJL, 891, L29

Jiménez-Ibarra, F., Muñoz-Darias, T., Wang, L., et al. 2018, MNRAS, 474, 4717

Kajava, J. J. E., Motta, S. E., Sanna, A., et al. 2019, MNRAS, 488, L18

Kawamuro, T., Negoro, H., Yoneyama, T., et al. 2018, ATel, 11399, 1

Kennea, J. A., Marshall, F. E., Page, K. L., et al. 2018, ATel, 11403, 1

Kojiguchi, N., Kato, T., Isogai, K., et al. 2019, ATel, 13066, 1

Marsh, T. R., Robinson, E. L., & Wood, J. H. 1994, MNRAS, 266, 137

Muñoz-Darias, T., Jiménez-Ibarra, F., Panizo-Espinar, G., et al. 2019, ApJL, 879, L4

Patterson, J. 2019, in Proc. 38th Annual Conf. Society for Astronomical Sciences, ed. R. K. Buchheim et al. (Rancho Cucamonga, CA: Society for Astronomical Sciences), 61, http://www.socastrosci.org/Publications.html

Patterson, J., Brincat, S., Stone, G., et al. 2018, ATel, 11756, 1

Peris, C. S., Vrtilek, S. D., Steiner, J. F., et al. 2015, MNRAS, 449, 1584

Shidatsu, M., Nakahira, S., Murata, K. L., et al. 2019, ApJ, 874, 183

Shidatsu, M., Ueda, Y., Nakahira, S., et al. 2013, ApJ, 779, 26

Steeghs, D., & Jonker, P. G. 2007, ApJL, 669, L85

Tassoul, J.-L. 1988, ApJL, 324, L71

Torres, M. A. P., Callanan, P. J., Garcia, M. R., et al. 2002a, ApJ, 569, 423

Torres, M. A. P., Casares, J., Jiménez-Ibarra, F., et al. 2019, ApJL, 882, L21

Torres, M. A. P., Casares, J., Martínez-Pais, I. G., et al. 2002b, MNRAS, 334, 233

Tucker, M. A., Shappee, B. J., Holoien, T. W. S., et al. 2018, ApJL, 867, L9

Warner, B. 1995, Cataclysmic Variable Stars, Vol. 28 (Cambridge: Cambridge Univ. Press)

Whitehurst, R., & King, A. 1991, MNRAS, 249, 25

Zahn, J.-P. 1977, A&A, 500, 121

Ziółkowski, J., & Zdziarski, A. A. 2018, MNRAS, 480, 1580

Zurita, C., Casares, J., Shahbaz, T., et al. 2002, MNRAS, 333, 791